Available online at www.sciencedirect.com
SCIENCE DIRECT®
ELSEVIER
International Journal of Solids and Structures 43 (2006) 1928–1945
INTERNATIONAL JOURNAL OF SOLIDS and STRUCTURES
www.elsevier.com/locate/ijsolstr

Reexamination of the solder ball shear test for evaluation of the mechanical joint strength

Jong-Woong Kim, Seung-Boo Jung *

Department of Advanced Materials Engineering, Sungkyunkwan University, 300 Cheoncheon-dong, Jangan-gu, Suwon 440-746, South Korea

Received 7 December 2004; received in revised form 1 June 2005
Available online 12 September 2005

Abstract

Ball shear tests were investigated in terms of the effects of test parameters, i.e., shear height and shear speed, with an experimental and non-linear finite element analysis for evaluating the solder joint integrity of area array packages. Two representative Pb-free solders were examined in this work: Sn–3.5Ag and Sn–3.5Ag–0.75Cu. The substrate was a common solder mask defined (SMD) type with solder bond pad openings of 460 μm in diameter. The microstructural investigations were carried out using scanning electron microscopy (SEM), and the intermetallic compounds (IMCs) were identified with energy dispersive spectrometry (EDS). Shear tests were conducted with the two varying test parameters. It was observed that increasing shear height at a fixed shear speed has the effect of decreasing shear force for both Sn–3.5Ag and Sn–3.5Ag–0.75Cu solder joints, while the shear force increased with increasing shear speed at fixed shear height. Shear heights that were too high had some negative effects on the test results such as unexpectedly high standard deviation values or shear tip sliding from the solder ball. Low shear height conditions were favorable for screening the type of brittle interfacial fractures or the degraded layers in the interfaces.

Keywords: Shear height; Shear speed; Finite element analysis; Pb-free solder; Ball grid array

1. Introduction

The proven ability of solder to connect components in electronic packages and printed circuit boards with good metallurgical bonding, and with the necessary mechanical strength and conduction properties, has resulted in its extensive application within the electronic industry, e.g., in PTH, SMT, and BGA

* Corresponding author. Tel.: +82 31 290 7359; fax: +82 31 290 7371.
E-mail address: sbjung@skku.ac.kr (S.-B. Jung).

0020-7683/$ - see front matter © 2005 Elsevier Ltd. All rights reserved.
doi:10.1016/j.ijsolstr.2005.07.014

applications. However, as the number of I/O pads increased and the size of solder joints decreased, i.e., the package density increased, solder joint reliability has become a more critical issue (Ho et al., 2004; Towashiraporn et al., 2004). Therefore, recent years have witnessed a large amount of researches concerning the properties of fine solder joints (Shiau et al., 2002; Kang et al., 2002; Yoon et al., 2004). However, most of these studies have been primarily concerned with discussions of the mechanical properties or the interfacial reactions between the solder and the metallization of the substrate. Researches into methods to test the mechanical strength of solder joints has been rare, though there is an emergent need to study the affordable test methods for package quality and reliability.

Currently, the most popular method to evaluate the strength of solder ball attachment is the ball shear test. Although this test is simple and convenient to implement, the details of performing the test have not yet been standardized for all uses of the ball shear test. The JEDEC (Joint Electronic Devices Engineering Council) BGA ball shear standard (JESD22-B117, 2002) prescribed that the gap between the edge of the shear ram and the surface of substrate should be larger than 0.05 mm and smaller than 25% of the ball height. However, this specification is published in terms of a generic procedure based on the case of common 1.27 mm pitch BGA packages, so cannot be applied with finer pitch and smaller solder ball attachments. In addition, another important ball shear test parameter, shear speed, is not fixed in the standard. The lack of specification necessary for shear speed may cause confusion and inconsistency in the comparison of the solder ball shear strengths characterized with different displacement rates.

A significant addition to the JESD22-B117 is the incorporation of the ball shear failure mode into the acceptance criteria. The primary impetus for including failure mode is to provide a mean for screening the type of brittle interfacial fractures caused by intermetallic compound (IMC) layers that are too thick. During soldering, the solder alloy melts and then reacts with the metallization of the substrate to form IMCs at the joining interface. While a thin IMC layer was formed, it is desirable to achieve a good metallurgical bond (Yoon et al., 2003). However, excessively thick reaction layers are very sensitive to stress and provide sites of initiation and paths of propagation for cracks, because the layer is brittle and a microstructural mismatch exists between the solder and pad metallization (Lee et al., 2003). However, during BGA ball shear testing, the side-walls of the SMD (Solder Mask Defined) area array bond pads tend to support the solder joint, which can alter the failure mode. Therefore, there is a reluctance to fully embrace the shear technique for monitoring susceptibility to brittle interfacial failures.

Huang et al. (2001) and Ricky Lee and Huang (2002) firstly studied the ball shear test in terms of the effects of shear speed and shear height. They employed both experimental and finite element analysis technique to investigate the effects and they found that the shear force increased with the shear speed and decreased with the shear height. However, they used a conventional Sn–37Pb solder and the finite element analysis was conducted with a NSMD (Non-Solder Mask Defined) type substrate. Therefore, the optimization of the shear test method for the whole kinds of BGA package was restrictively discussed. Huang et al. (2002) also reported progressive failure mechanism of solder balls during the ball shear test with experimental investigation. They revealed the failure mechanisms with 3 different failure modes in this study. Kim et al. (2003), Kim and Jung (2004) reported that the shear speed effects in the shear test of In–48Sn which has a low melting temperature and Sn–Ag and Sn–Ag–Cu Pb-free solder balls which have high melting temperatures using similar experimental and simulation techniques with Huang et al. (2001). They revealed that the effect of shear speed on the shear force of the solder joints highly increased with decreasing melting temperature of solder balls. However, the effect of shear height was not included, and the optimization of the test methods was not discussed.

Therefore, the objectives of this study are to evaluate the effect of important shear test parameters, such as shear height and shear speed, and recommendations for getting favorable test results. Two kinds of representative lead free solders, Sn–3.5Ag and Sn–3.5Ag–0.75Cu solders were used to observe the effects of the above parameters under shear testing. Both experimental investigation and non-linear finite element analysis using elastic-viscoplastic constitutive model were carried out. Two finite element analysis tools, the

Surface Evolver developed by Brakke and modified by Chiang and Yuan and the ANSYS were used to analyze the solder ball joints. Analytical stress and averaged equivalent plastic strain analyses were performed to interpret the failure mechanisms.

2. Experimental and analysis procedures

2.1. Experimental procedures

The BGA solders used in this study were Sn–3.5Ag and Sn–3.5Ag–0.75Cu (in mass %). Solder balls of these materials had a diameter of 500 μm. The substrate was an SMD type bismaleimide triazine (BT) laminate with subsurface solder bond pads whose nominal size and shape were defined through a circular opening of 460 μm in diameter with 1 mm pitch. The pads comprised electroplated Au over Ni on an underlying Cu pad with thicknesses of 0.5 and 7.0 μm, respectively. The Sn–3.5Ag and Sn–3.5Ag–0.75Cu solder balls were bonded to the BT substrate in a reflow process employing RMA flux in an IR four zone reflow machine (RF-430-N2, Japan Pulse Laboratory Ltd. Co.) with a maximum temperature of 255 °C for 60 s. To investigate the effect of shear height on the fracture mode of the joints with relatively thick IMC layers, an aging condition of 180 °C for 200 h was employed. Microstructural observations were conducted using scanning electron microscopy (SEM) and the compositions of the resulting IMCs were determined using energy dispersive spectrometry (EDS). Shear tests were conducted using a global bond tester (Dage-4000 s, Richardson Electronics Ltd.) under various test conditions. The shear test conditions used in this work are given in Tables 1 and 2. The fracture mode of each test site was examined after shear testing to evaluate the mode of failure.

2.2. Finite element analysis

The reflow geometry of the solder ball was predicted using the Surface Evolver program. The Surface Evolver is an energy-based method for predicting the shape of a liquid body. To simulate the geometric shape of a liquid body, the Surface Evolver deconstructs the initial simplex surface of a liquid body into a set of triangular facets and then iterates these facets toward a minimal energy equilibrium situation using the gradient descent method. In a situation of static equilibrium, the total energy of a liquid body is generally comprised of three major energy portions, e.g., surface tension energy, gravitational energy, and external energy related to changes in body volume (Zhao et al., 2000; Chiang and Yuan, 2001). Fig. 1 shows the general cross-sectional view of a reflowed BGA solder joint and the 3-dimensional (3-D) finite element model predicted by the Surface Evolver. To confirm the accuracy of the geometric predictions, actual measurements of solder balls were compared to the prediction. Table 3 compares the solder ball diameter,

Table 1
Examined shear height conditions

Shear speed (μm/s)	Shear height (μm)					
200	10	30	50	70	90	120

Table 2
Examined shear speed conditions

Shear height (μm)	Shear speed (μm/s)						
50	10	50	100	200	300	400	500

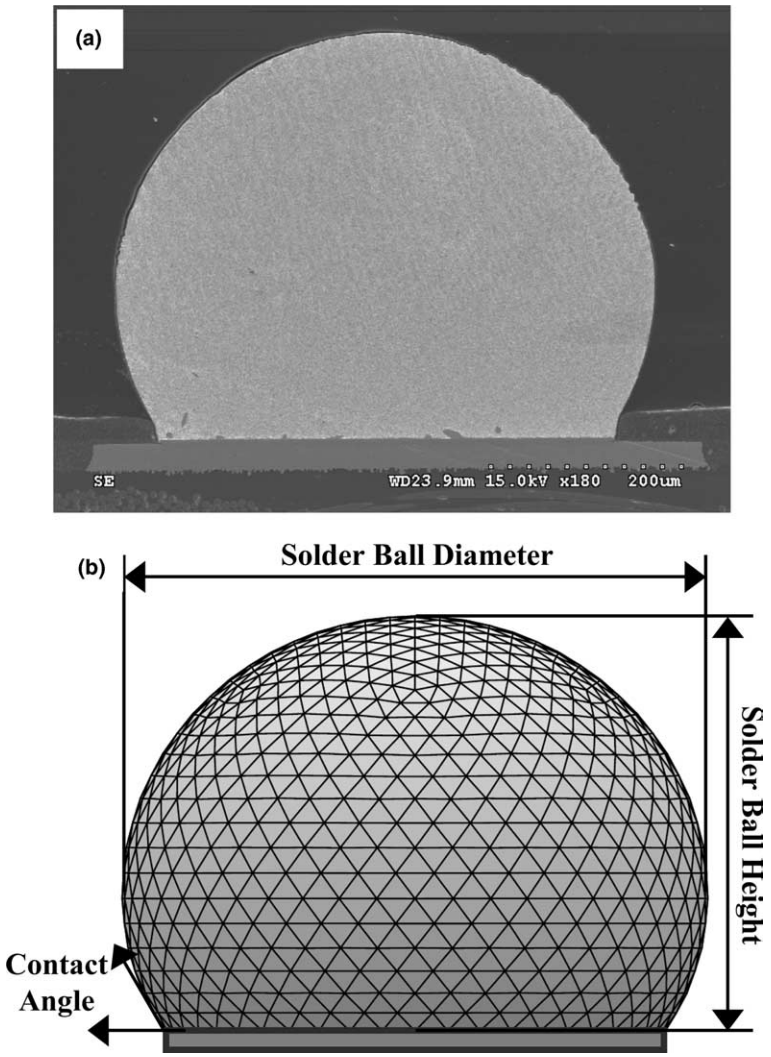

Fig. 1. Geometric profile comparison between actual (a) and predicted solder ball attachment (b).

Table 3
Comparison of solder ball shape between actual and predicted model

	Actual model	Predicted model
Solder ball diameter (μm)	553.9	554.7
Solder ball height (μm)	394.3	392.1
Contact angle (degree)	58.7	57.2

height and contact angle of the actual solder ball with the predicted solder ball dimensions, revealing a close agreement between the Surface Evolver prediction and the actual values.

The key points of the solder ball surface were obtained from the Surface Evolver predictions using a curve-fitting program, and then used to construct the solder ball model in ANSYS software. In order to

reduce the time taken for analysis, 2-D elastic-viscoplastic finite element simulation methodologies were utilized to predict the effect of ball shear parameters on shear force. The components of the finite element simulation included a reflowed solder ball, the BT substrate, the subsurface Cu pad and the electroplated Ni layer. The shear ram was considered as a rigid body. The surface-to-surface target element (TARGE169) and the contact element (CONTA172) were employed to simulate the contact between the shear ram and the solder ball. Since this modeling was a 2-D analysis, a scale factor of effective thickness was calculated and applied for getting the "shear force" instead of "shear force per unit thickness". We calculated the effective thickness at 320 μm with comparison between experimental shear force and simulated shear force of a base case condition (shear speed of 100 μm/s, shear height of 50 μm). The calculating method of the effective thickness was firstly suggested by Ricky Lee and Huang (2002), and thus, the detailed procedures could be found in their paper. Fig. 2(a) and (b) show the overall 2-D finite element model for the ball shear test and the magnified view near the left side of the Ni layer, respectively.

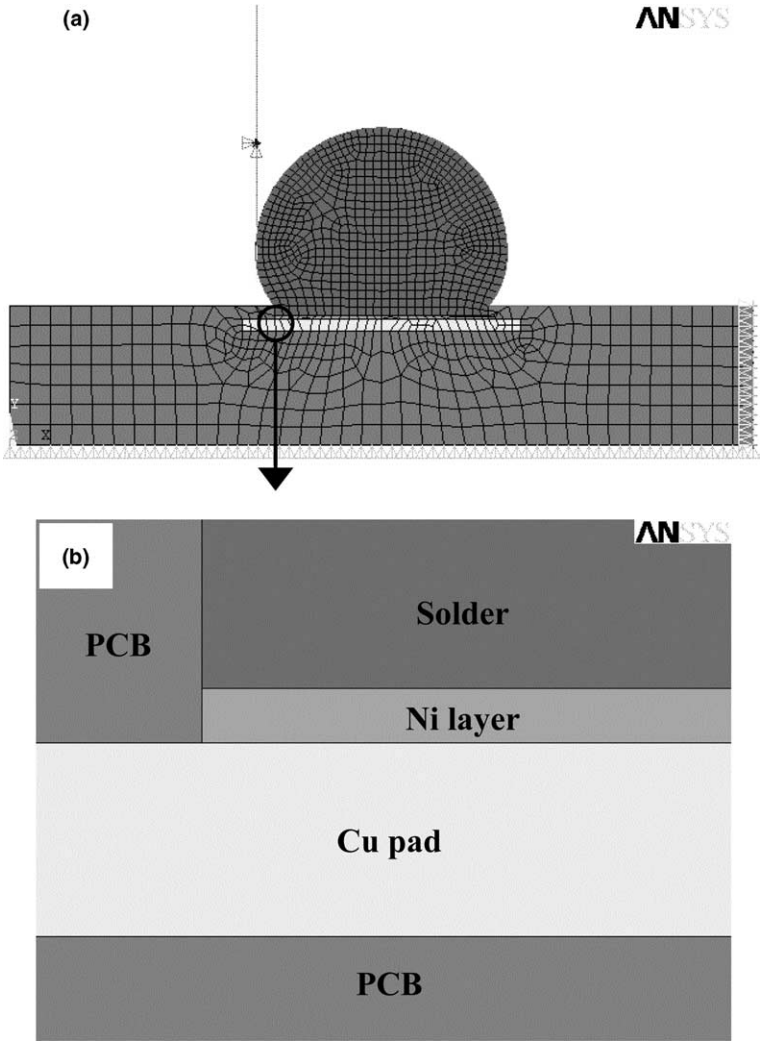

Fig. 2. Finite element model for the ball shear test (a) and magnified view near the Ni layer (b).

Because the test temperature was in excess of a homologous temperature of 0.5, linear and non-linear, time dependent and independent material properties were incorporated in the finite element model (Amagai, 1999; Lin et al., 2002; Lau and Ricky Lee, 2002). In the present work, Anand viscoplastic constitutive model was employed to represent the viscoplastic behavior of the solders. The Anand model was firstly suggested by Anand (1982, 1985) to be used for analyzing the rate-dependent deformation of metals at temperatures in excess of a homologous temperature of 0.5. Then, this model was found to be very useful for representation of the viscoplastic properties of the solder materials, therefore, there are sizable researches employing the Anand model for the analysis of the solder deformation behaviors. The detailed description of the Anand model could be found in his studies (1982; 1985), and thus only leaded equations which are consisting of flow and evolution equations are introduced in this study. The Anand model is a unified framework for the viscoplastic behavior of solder materials, in which plasticity and creep are unified and described by the same set of flow and evolutionary equations. However, the Anand model is only available for VISCO10X elements in ANSYS causing a convergence more difficult and time consuming. Therefore, the following steps were evolved to extract only steady state creep behavior from the Anand model.

The following functional form for the flow equation of the Anand model was selected to accommodate the strain rate dependence on stress at constant structure:

$$\frac{d\varepsilon_p}{dt} = A \exp\left(-\frac{Q}{RT}\right)\left[\sinh\left(\xi\frac{\sigma}{s}\right)\right]^{1/m} \tag{1}$$

where $d\varepsilon_p/dt$ is the inelastic strain rate, A is the pre-exponential factor, Q is the activation energy, R is the gas constant, T is the absolute temperature, ξ is the multiplier of stress, σ is the applied stress, s is a single scalar as an internal variable to represent the averaged isotropic resistance to plastic flow, and m is the strain rate sensitivity of stress.

The evolution equation for the internal variable s is derived by

$$\frac{ds}{dt} = \left[h_0\left|1-\frac{s}{s^*}\right|^a \times \left\{\left(1-\frac{s}{s^*}\right)\Big/\left|1-\frac{s}{s^*}\right|\right\}\right] \times \frac{d\varepsilon_p}{dt}, \quad a > 1 \tag{2}$$

with

$$s^* = \hat{s}\left[\frac{d\varepsilon_p/dt}{A}\exp\left(\frac{Q}{RT}\right)\right]^n \tag{3}$$

where h_0 is the hardening/softening constant, s^* is the saturation value of s, a is the strain rate sensitivity of hardening/softening, $\hat{s}$ is the coefficient for the saturation deformation resistance, and n is the strain rate sensitivity for the saturation value of deformation resistance.

The flow equation of the Anand model follows the same hyperbolic sine form of the secondary creep law with modification of the internal state variable as denominator in the stress term, together with providing an evolution equation for the state variable. Steady state plastic flow occurs when the deformation resistance s equals the saturation value s^*. At that point, the evolution equation can be removed and there is no hardening/softening effect, the hardening/softening constant is given a value of zero, i.e. $h_0 = 0$ and its strain rate sensitivity $a = 1$. The strain rate sensitivity for s^* is also set to zero, i.e. $n = 0$, resulting in the parameters s_0 and $\hat{s}$ processing the same value as s^*.

Thereafter, the Anand model is simplified to the hyperbolic sine creep form, resulting in the following steady state creep equation.

$$\frac{d\varepsilon_p}{dt} = A \exp\left(-\frac{Q}{RT}\right)[\sinh(\alpha\sigma)]^{1/m} \tag{4}$$

where $d\varepsilon_p/dt$ is the steady state creep strain rate, and α is the stress level at which the power law dependence breaks down. It should be noted that Eq. (4) is exactly the same form of input for implicit creep model

Table 4
Linear elastic material properties for BGA assemblies

Materials	Young's modulus (MPa)	Poisson's ratio	Density (g/cm^3)
Sn–3.5Ag	49,800	0.40	7.5
Sn–3.5Ag–0.75Cu	54,900	0.40	7.5
Cu	117,000	0.34	8.9
Ni	213,000	0.31	8.9
BT substrate	14,000	0.39	1.2

Table 5
Input parameters for steady state creep analysis

	A (1/s)	α (1/kPa)	m	Q/R (K)
Sn–3.5Ag	9.00E5	4.5E−4	0.182	8,690
Sn–3.5Ag–0.75Cu	4.61E6	3.7E−5	0.162	8,400

(TBOPT = 8) of ANSYS, release 6.1. This creep option was combined with the Multilinear Isotropic (MISO) hardening using von Mises plasticity to represent the viscoplastic properties of the solder material. The linear elastic material properties and steady state creep constants are given in Tables 4 and 5, respectively. The steady state creep constants were those converted from the Anand model constants (Amagai et al., 2002; Lau, 1995).

3. Results and discussion

In determining the failure mode of the solder ball under shear testing, analysis of the averaged incremental equivalent plastic strain was performed, because the load on the pad site of the solder ball during a shear test is a mixture of tensile, shear and compressive forces, especially at the corners of the solder (Chang and Chiang, 2004). Fig. 3(a) and (b) plot the distributions of the averaged equivalent plastic strain for the base case, shear height of 50 μm and shear speed of 200 μm/s, of the Sn–3.5Ag and Sn–3.5Ag–0.75Cu joints, respectively. From Fig. 3, the region of high plastic strain in the solder ball was found to be near the contact point between the shear ram and the solder, and had expanded through the solder in parallel to the substrate. This implies a strong likelihood of crack initiation and growth through this region. The cross-sectional views of the solder balls after the shear testing are shown in Fig. 4. Comparing Fig. 3 with Fig. 4, the shear failure modes of the solder ball joints, determined by computational analysis, correlate well with the actual solder ball failure modes under shear testing.

Fig. 5(a) and (b) show the force–displacement curves from the experiment and modeling computations for the base condition, corresponding to Sn–3.5Ag and Sn–3.5Ag–0.75Cu, respectively. The maximum shear force of the Sn–3.5Ag–0.75Cu solder joint was found to be higher than that of the Sn–3.5Ag solder joint, and this is consistent with the results from the previous studies (Li et al., 2001). The difference in shear force between the two solders is mainly considered to be due to the Cu solution in the Sn matrix of the Sn–3.5Ag–0.75Cu solder. The graphs from the experiment and modeling both show similar concave down behavior except for the initial stage of the curves where the experimental curves show a region curving upward which seems to be mainly due to the experimental errors such as flux residues. Alternately, the reflowed ball shape may produce a concave up Hertzian loading curve characteristic of increasing contact area with the ram of the shear tester. From the two results mentioned above, it can be concluded that the finite element analysis used in this study is reasonably reliable.

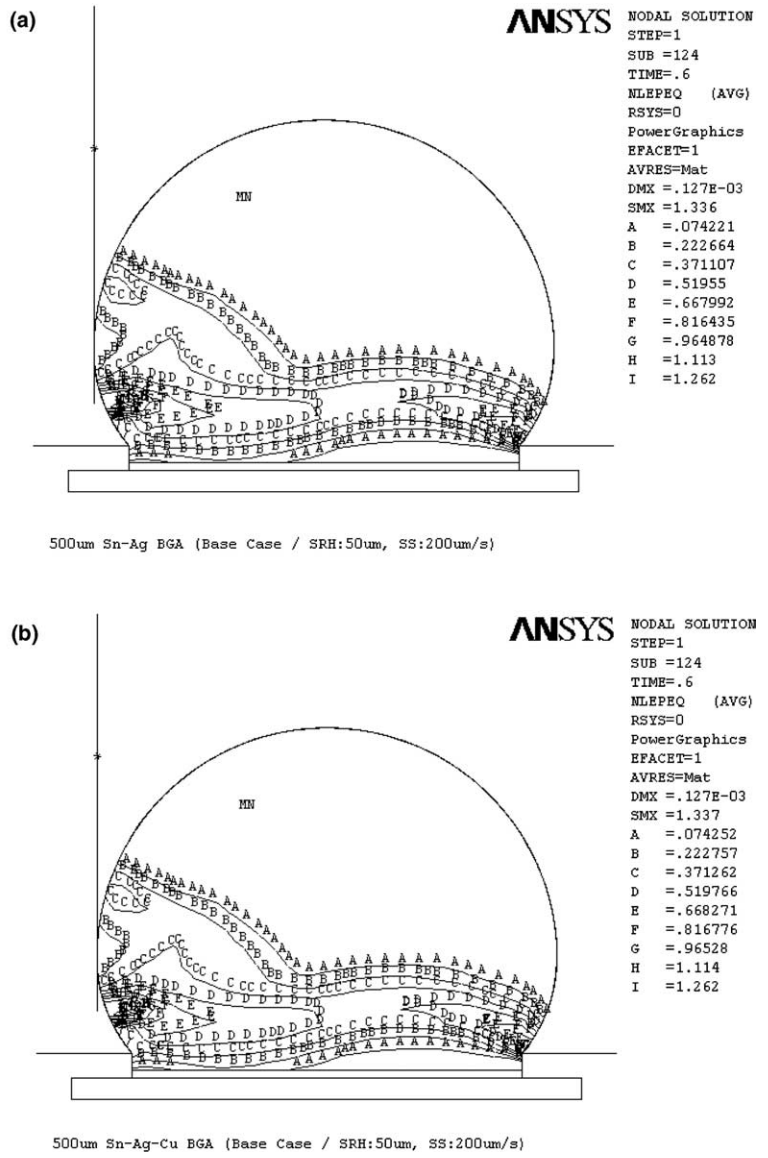

Fig. 3. Contour plots of averaged equivalent plastic strain analysis in the base case condition (shear height: 50 μm, shear speed: 200 μm/s): (a) Sn–3.5Ag, (b) Sn–3.5Ag–0.75Cu.

Fig. 6(a) and (b) show back scattered electron (BSE) micrographs for the interfaces between the two kinds of solders and the Au/Ni electroplated layer on the Cu pad. Only a Ni–Sn IMC was formed between the Sn–3.5Ag and the Ni layer, while the Au layer appears to have dissolved into the liquid solder leaving no observable Au at the interface. From the EDS compositional analyses, the Ni–Sn IMC was observed to be indicating Ni_3Sn_4 phase. The thickness of the Ni_3Sn_4 IMC layer was approximately 1.1 μm. In the Sn–3.5Ag–0.75Cu solder and Au/Ni/Cu pad reaction, a continuous layer of $(Ni_{1-x}Cu_x)_3Sn_4$ and discontinuous $(Cu_{1-y}Ni_y)_6Sn_5$ particles could be seen, as shown in Fig. 6(b). The compositions of these phases, determined by EDS, were found to be $(Ni_{0.72}Cu_{0.28})_3Sn_4$ and $(Cu_{0.66}Ni_{0.34})_6Sn_5$, respectively. Some Ag_3Sn IMCs were

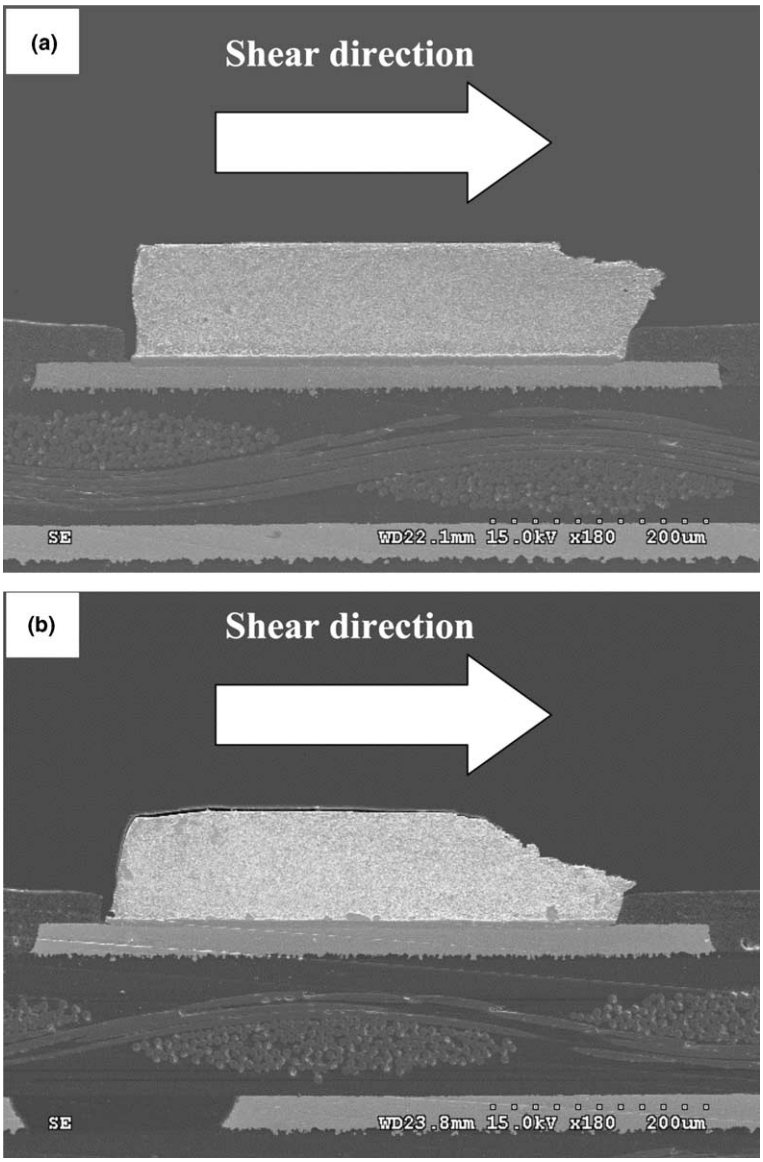

Fig. 4. Cross-sectional views after ball shear test in the base case condition (shear height: 50 μm, shear speed: 200 μm/s): (a) Sn–3.5Ag, (b) Sn–3.5Ag–0.75Cu.

distributed inside the two solders, and could be considered an influential factor controlling the mechanical properties of the solders (Kim and Jung, 2004). An IMC layer that is too thick is sensitive to stress and provides sites of initiation and paths of propagation for cracks, because the layer is brittle and a microstructural mismatch exists between the solder and metallization. Therefore, the growth of the IMC layer can lead to the degradation of solder ball shear strength. For this reason, from the perspective of the reliability of electronic packages, it is very important to screen the brittle interfacial fractures or to identify weak interfaces in solder joints when high temperature storage, burn-in, or extended bake-out cause thick IMC layers.

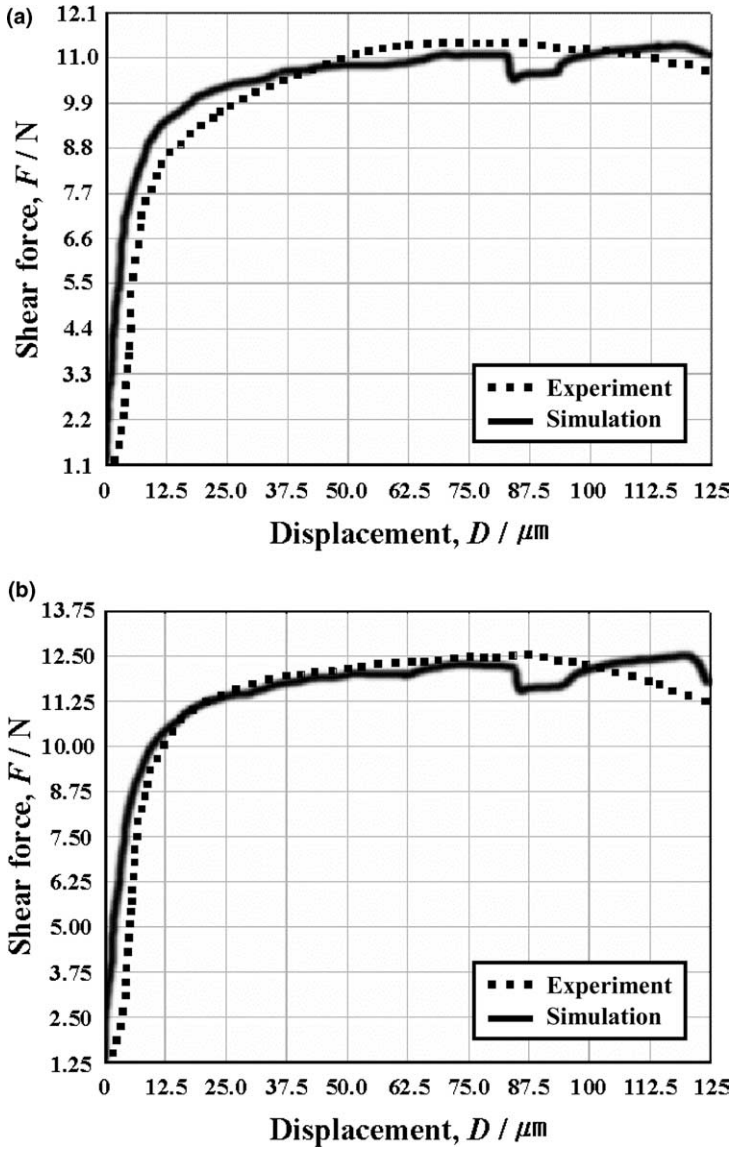

Fig. 5. Force–displacement curves in the base case condition (shear height: 50 μm, shear speed: 200 μm/s): (a) Sn–3.5Ag, (b) Sn–3.5Ag–0.75Cu.

Fig. 7(a) and (b) show the shear force variations of the experiment and computational modeling under increasing shear height, for both the Sn–3.5Ag and Sn–3.5Ag–0.75Cu solders, respectively. Experimentally, for each test condition, 30 solder balls were placed under shear stress until their failure point was reached. The shear force required to achieve failure decreased with increasing shear height and reached the minimum value at the highest ram height. This implies that the resistance to plastic deformation is increased by increasing contact area between the shear ram and bulk solder. In the same manner, the computational results indicate that the shear force decreased with increasing shear height. The physical results observed and the mathematical calculations are in qualitative agreement. However, it should also be noted that, in the

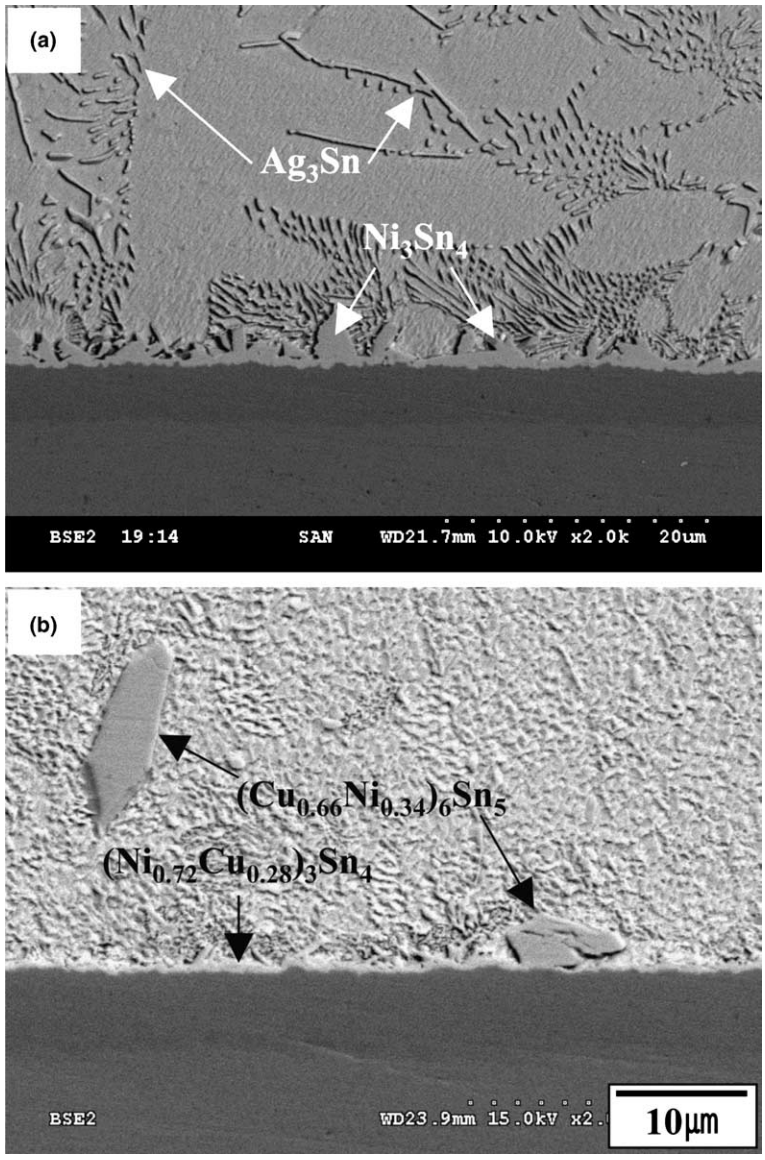

Fig. 6. SEM micrographs of Sn–3.5Ag (a), and Sn–3.5Ag–0.75Cu (b) solder joint interface.

cases involving a shear height of over 70 μm, both the mismatches between the experimental and computational results and standard deviation values from the experimental results increased. These were because the contact area between the shear ram and solder was so confined, while the local deformation in the solder had become too severe (the edge of the shear ram cuts deeply into the solder ball due to the high ram height). In addition, when the shear height was high the shear probe frequently slides off from the solder ball. Consequently, when the shear probe was dropped from higher heights, the experimental results obtained for shear force were more susceptible to the experimental factors such as the indefinite quantity of the solder applied to the pad which results in different ball shapes, flux residues on the ball surface,

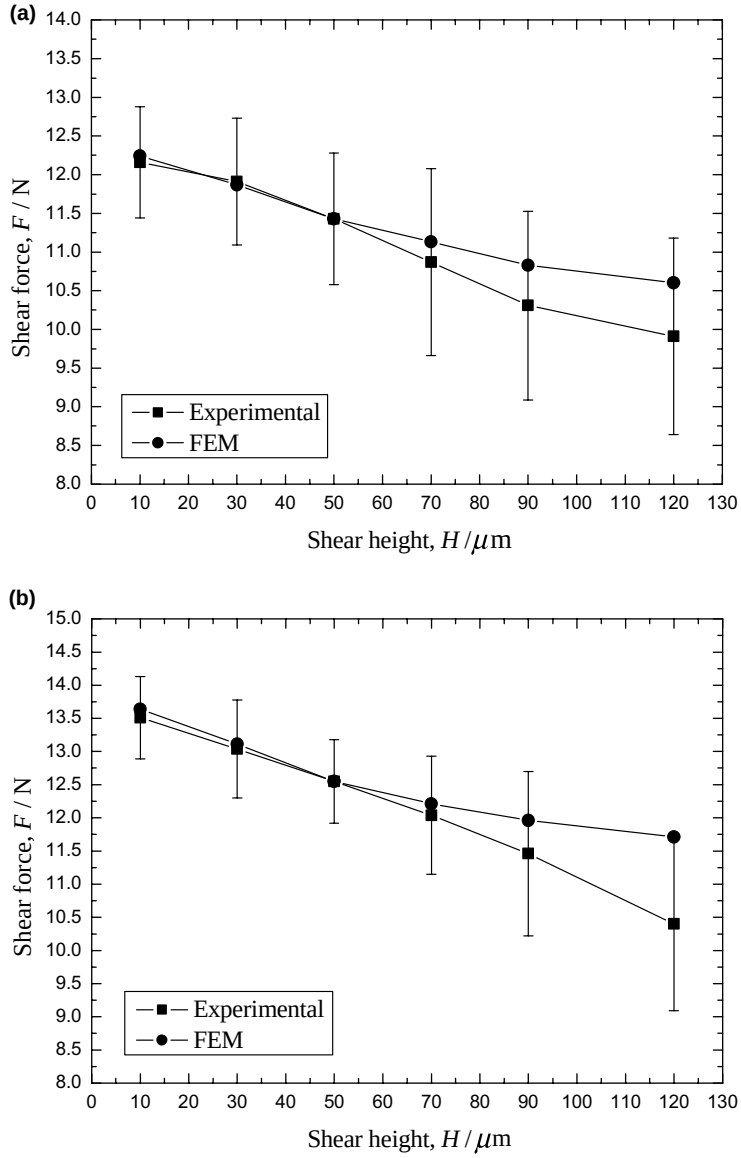

Fig. 7. Shear force variations with increasing shear height: (a) Sn–3.5Ag, (b) Sn–3.5Ag–0.75Cu.

compliance of the shear test fixturing and oxidation at the BGA surface. From engineering perspective, too high shear heights should not be included in the test conditions.

Fig. 8 shows the distributions of averaged equivalent plastic strain and the fracture surfaces of the test specimens after shear testing of Sn–3.5Ag–0.75Cu solder joints. Fig. 8(a) and (b) show samples with a shear height of 10 μm and a shear speed of 200 μm/s, while Fig. 8(c) and (d) show samples with a shear height of 120 μm and a shear speed of 200 μm/s. As shown in the figures, the strain is very densely accumulated in the right above the Ni layer for samples with a shear height of 10 μm, while the strain is spread out in the upper region of the solder for samples with a shear height of 120 μm. This is well correlated with

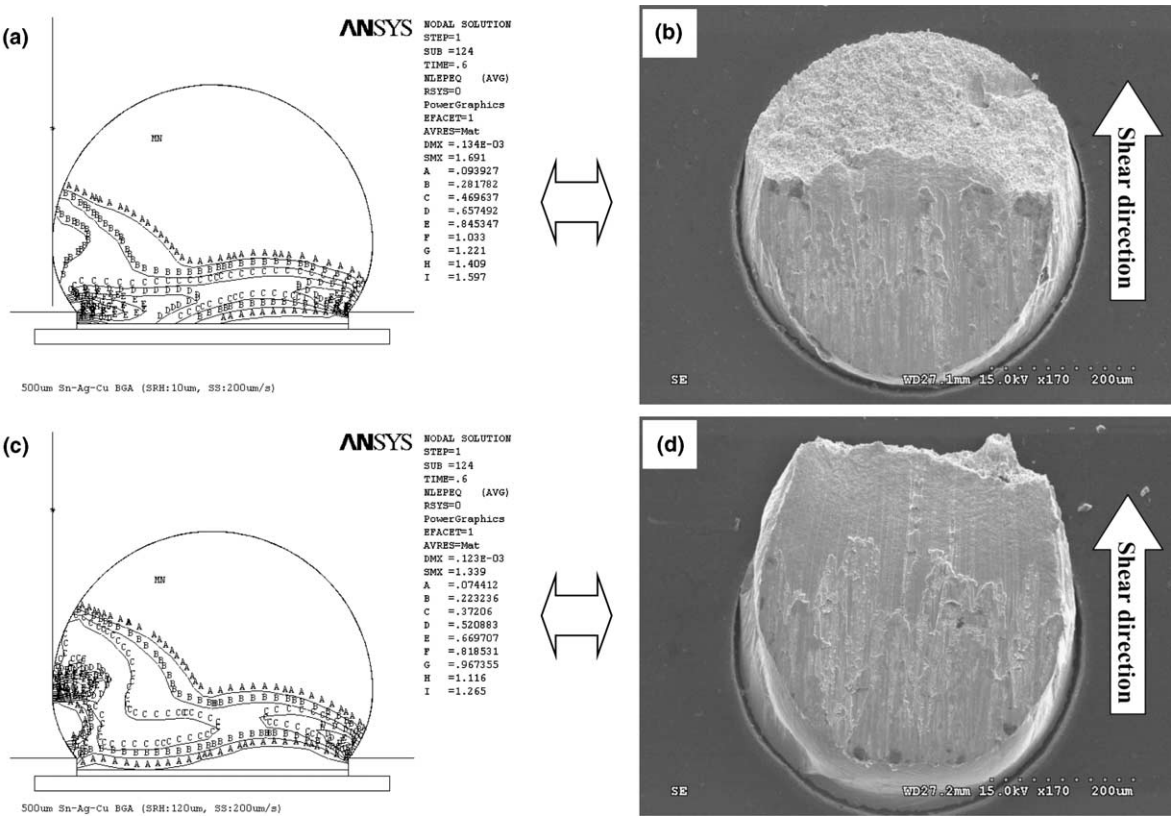

Fig. 8. Distributions of averaged equivalent plastic strain and fracture surfaces after shear test of Sn–3.5Ag–0.75Cu solder joints: (a, b) 10 μm of shear height, (c, d) 120 μm of shear height.

the corresponding fracture surfaces shown in Fig. 8(b) and (d). Furthermore, the maximum value of strain shown in Fig. 8(a) is higher than that shown in Fig. 8(c). Therefore, it could be deduced that, if the IMC layer between the solder and pad metallization is too thick, brittle interfacial failure can be more easily achieved under conditions with lower shear height.

Fig. 9 presents the von Mises stress distributions within the Cu pad and Ni layer. The figure indicates that the application of shear loads to a multi-phase structure results in the formation of a singularity phenomenon, i.e., a stress concentration, at the corner of the common boundary of the two different materials. This is due to the phase discontinuity which occurs at this boundary. However, the location of the maximum stress is different between the two samples examined with varying shear heights of 10 μm and 120 μm. The maximum stress region is located in the left corner of the Ni layer when the shear height is 10 μm, while the stress is concentrated in the right corner of the Ni layer that could not be the initiation of the failure path when the shear height is 120 μm. This means that the cases with lower shear height could screen the type of brittle interfacial fractures or the degraded layers in the interfaces more easily. Even though the maximum stress occurs within the Ni layer, cracking does not readily occur near this layer since the strengths of the IMCs and Ni are greater than the strength of the solder. Accordingly, it could be said that when the thickness of the interfacial IMC layer is thicker, brittle interfacial failure can be achieved with lower shear heights. It should also be noted that the stress value on the Ni layer in the shear condition of low shear height is larger than that of the high shear height. This means that more large stress

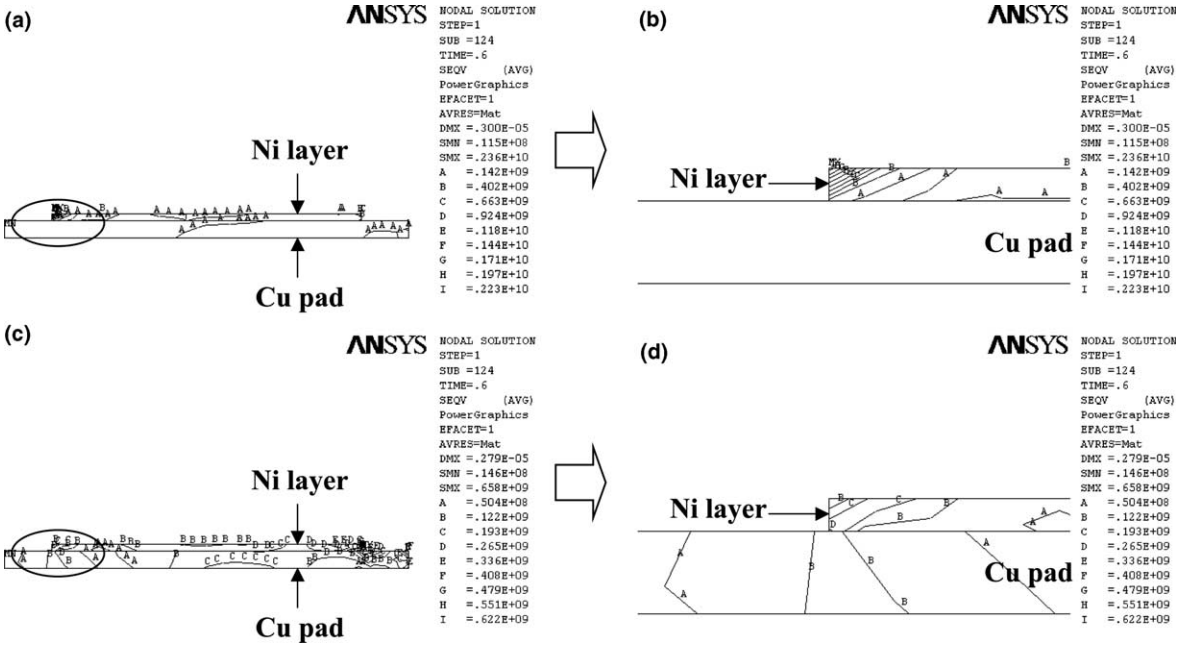

Fig. 9. Von Mises stress contours within the Cu pad and Ni layer: (a, b) 10 μm of shear height, (c, d) 120 μm of shear height.

concentration was occurred at the lower shear height, and this is well explaining why the shear force decreased with increasing shear height.

Fig. 10 shows the general cross-sectional view of the aged Sn–3.5Ag–0.75Cu solder joints after shear testing using a shear height of 10 μm and a shear speed of 200 μm/s. The aging conditions for the sample in

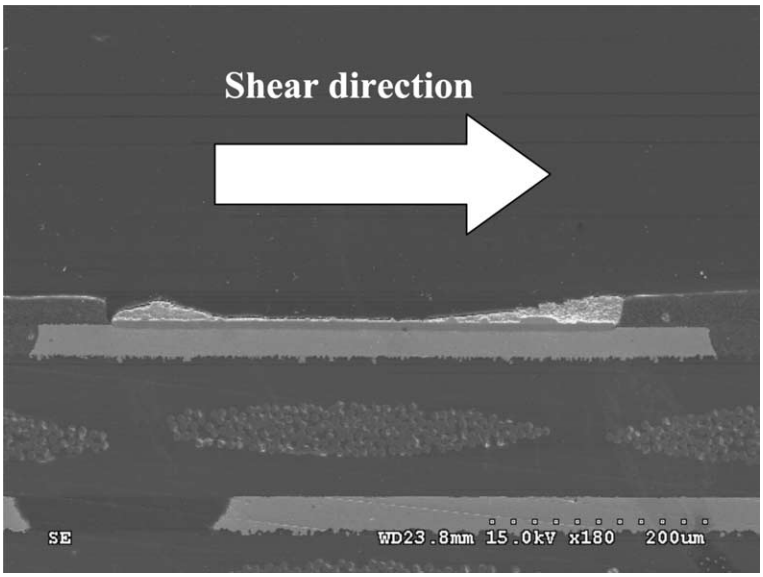

Fig. 10. Cross-sectional view after shear test of the aged specimen in the condition of 10 μm shear height.

Fig. 10 were 180 °C temperature with an aging time of 200 h. As shown in the figure, the failure type was a mixed mode of ductile and brittle. About 70% of the specimens exhibited this mixed mode of failure, while a very limited number of the specimens resulted in mixed failure mode under other test conditions. This correlates very well with the simulation results described above.

The shear force variations of both the actual experimental results and the computational modeling under increasing shear speed are shown in Fig. 11. Shear force is proportional to shear speed and reaches a maximum value at the highest shear speed in both the experimental and computational results. This means that the increase in shear force with increasing shear speed is a direct consequence of the material properties

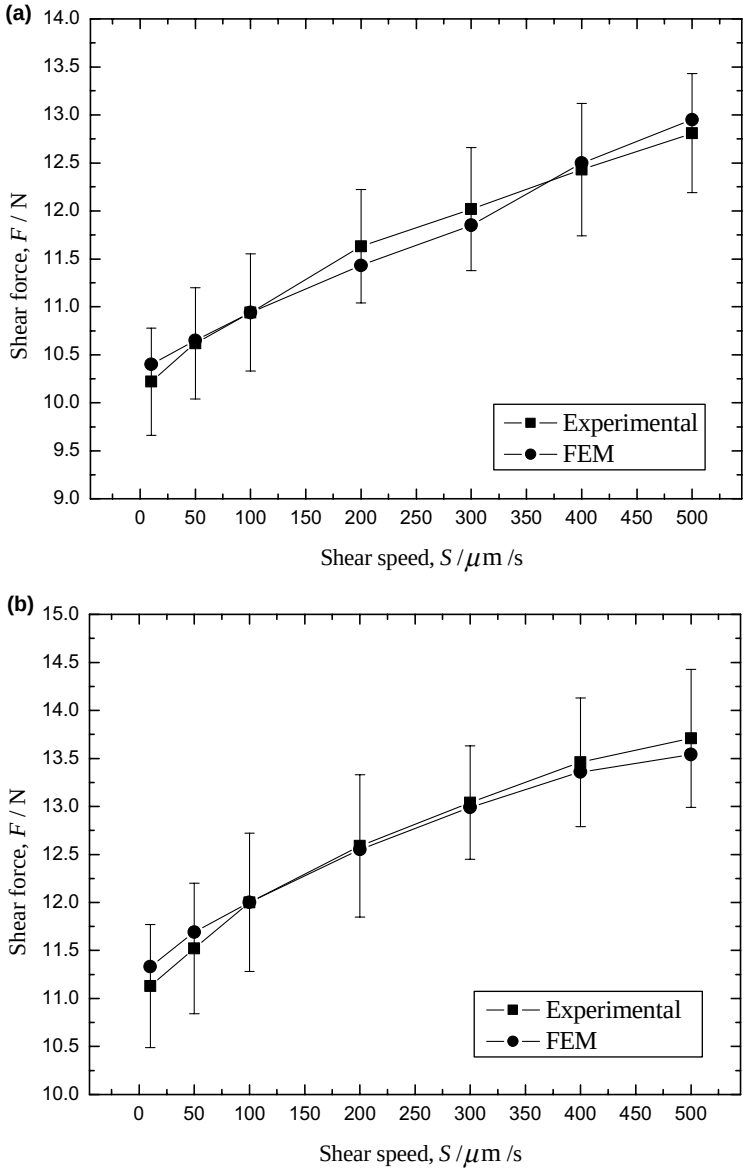

Fig. 11. Shear force variations with increasing shear speed: (a) Sn–3.5Ag, (b) Sn–3.5Ag–0.75Cu.

including both time-independent plastic hardening and time-dependent creep. According to Nadai's mathematical analysis, a general relationship between flow stress and strain rate, at constant strain and temperature, can be expressed by (Dieter, 1988; Nadai, 1950)

$$\sigma = C\left(\frac{\mathrm{d}\varepsilon}{\mathrm{d}t}\right)^{s}\Bigg|_{\varepsilon,T} \tag{5}$$

where s is known as the strain-rate sensitivity and C is a constant. The exponent s can be obtained from the slope of a plot of $\log\sigma$ vs. $\log(\mathrm{d}\varepsilon/\mathrm{d}t)$. In ordinary metals with a high melting point, the strain-rate sensitivity

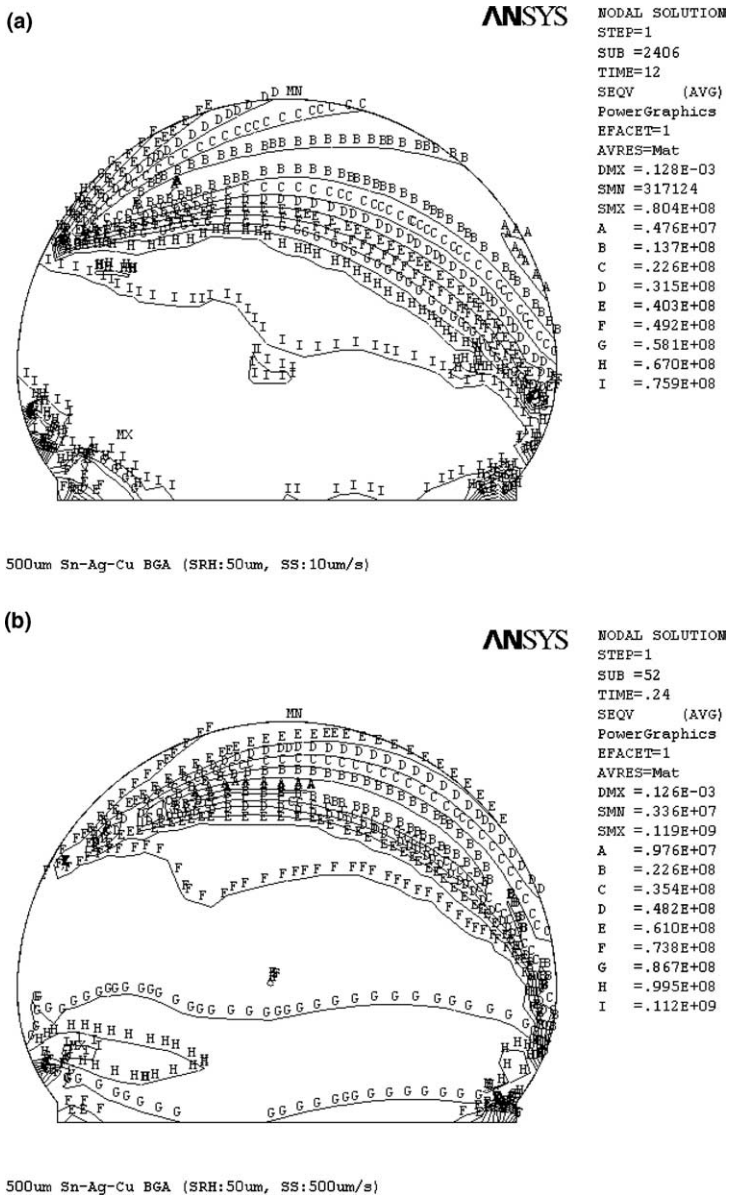

Fig. 12. Von Mises stress contours within the solder: (a) 10 μm/s of shear speed, (b) 500 μm/s of shear speed.

(s) is quite low (<0.1) at room temperature, but s increases with temperature, especially at temperatures above a homologous temperature of 0.5. Because room temperature is higher than halfway point of the solder melting point on the absolute temperature scale, the strain rate or displacement rate is very important to the stress flow properties. According to previous research, the shear force of In–48Sn solder which has a low melting point increased from approximately 1.6 to 3.0 N with shear speeds ranging from 10 to 700 μm/s, i.e., an approximately 88% increase in shear force (Kim et al., 2003). This adds reinforcement to the theory previously mentioned.

Fig. 12 shows the von Mises stress contour analyses of the Sn–3.5Ag–0.75Cu solder for the two test conditions which were shear speed of 10 μm/s and 500 μm/s with a fixed shear height of 50 μm. The region of highest stress in the solder ball included fracture locations which were shown in Figs. 4 and 8. This implies that ball shear mode is also closely related to the region of high von Mises stress contours. In the figure, the von Mises stress values increased with increasing shear speed, giving rise to the increasing ball shear forces as reported in Fig. 11.

4. Conclusion

An analysis into the test method for determining the strength of Pb-free BGA solder joints was carried out. The results have been used to draw the following conclusions.

1. The shape of the reflowed solder ball was successfully predicted using an energy-based simulation tool, i.e., Surface Evolver. The results from the simulation, such as the averaged equivalent plastic strain and the force–displacement curves, indicated that the finite element analysis used in this study was reasonably reliable.
2. Only a Ni_3Sn_4 IMC layer was formed at the interface between the pad metallization and Sn–3.5Ag solder, while a continuous layer of $(Ni_{0.72}Cu_{0.28})_3Sn_4$ and some IMC particles of $(Cu_{0.66}Ni_{0.34})_6Sn_5$ were found between the pad and Sn–3.5Ag–0.75Cu solder.
3. It was found that increasing shear height, with a fixed shear speed, had the effect of decreasing the shear force for both Sn–3.5Ag and Sn–3.5Ag–0.75Cu solder joints. These results were considered to be due to the increasing contact area between the shear ram and bulk solder.
4. Shear heights that were too high tended to have negative effects on the test results, e.g., unexpectedly high standard deviation values or cases where the shear tip slide from the solder ball. Therefore, shear test conditions involving shear heights greater than 20% of the solder ball height should be avoided.
5. From the computational results, the relatively low shear height conditions were favorable for screening the type of brittle interfacial fractures or the degraded layers in the interfaces. This concurred with the experimental results performed on sufficiently aged specimens.
6. The shear force increased with increasing shear speed for conditions involving a fixed shear height of 50 μm. The shear force of the two solder joints increased approximately 30% when the shear speed was increased from 10 to 500 μm/s. These results follow the same trends as results found in other researches.

Acknowledgement

The present work was carried out with the support of a Standardization-Technology-Development-Program (Project No. 10012693) of the Korea Ministry of Commerce, Industry and Energy.

References

Amagai, M., 1999. Characterization of chip scale packaging materials. Microelectronics Reliability 39, 1365–1377.

Amagai, M., Watanabe, M., Omiya, M., Kishimoto, K., Shibuya, T., 2002. Mechnical characterization of Sn–Ag based lead-free solders. Microelectronics Reliability 42, 951–966.

Anand, L., 1982. Constitutive equations for the rate-dependent deformation of metals at elevated temperatures. Transactions of the ASME 104, 12–17.

Anand, L., 1985. Constitutive equations for hot working of metals. Journal of Plasticity 1, 213–231.

Chang, K.C., Chiang, K.N., 2004. Improvements of solder ball shear strength of a wafer-level CSP using a novel Cu stud technology. IEEE Transactions on Components and Packaging Technologies 27, 373–382.

Chiang, K.N., Yuan, C.A., 2001. An overview of solder bump shape prediction algorithms with validations. IEEE Transactions on Advanced Packaging 24, 158–162.

Dieter, G.E., 1988. Mechanical Metallurgy. McGraw-Hill, New York.

Ho, S., Wang, G., Ding, M., Zhao, J., Dai, X., 2004. Reliability issues for flip-chip packages. Microelectronics Reliability 44, 719–737.

Huang, X., Ricky Lee, S.W., Yan, C.C., 2002. Experimental investigation on the progressive failure mechanism of solder balls during ball shear test. In: Proceedings of the 2002 Electronic Components and Technology Conference. IEEE, San Diego, pp. 968–973.

Huang, X., Ricky Lee, S.W., Yan, C.C., Hui, S., 2001. Characterization and analysis on the solder ball shear testing conditions. In: Proceedings of the 2001 Electronic Components and Technology Conference. IEEE, Orlando, pp. 1065–1071.

JESD22-B117, JEDEC Solid State Technology Association, 2002.

Kang, S.K., Choi, W.K., Yim, M.J., Shih, D.Y., 2002. Studies of the mechanical and electrical properties of lead-free solder joints. Journal of Electronic Materials 31, 1292–1303.

Kim, J.W., Jung, S.B., 2004. Experimental and finite element analysis of the shear speed effects on the Sn–Ag and Sn–Ag–Cu BGA solder joints. Materials Science and Engineering A 371, 267–276.

Kim, J.W., Kim, D.G., Koo, J.M., Jung, S.B., 2003. Effect of shear speed on the shear force of low melting point BGA solder joints. In: Proceedings of the 5th International Conference on Electronics Materials and Packaging. IEEE, Singapore, pp. 282–288.

Lau, J.H., 1995. Ball Grid Array Technology. McGraw-Hill, New York.

Lau, J.H., Ricky Lee, S.W., 2002. Modeling and analysis of 96.5Sn–3.5Ag lead-free solder joints of wafer level chip scale package on buildup microvia printed circuit board. IEEE Transactions on Electronics Packaging Manufacturing 25, 51–58.

Lee, H.T., Chen, M.H., Jao, H.M., Liao, T.L., 2003. Influence of interfacial intermetallic compound on fracture behavior of solder joints. Materials Science and Engineering A 358, 134–141.

Li, L., Jang, J.W., Allmen, B., 2001. Shear property and microstructure evaluation of Pb-free solder bumps under room temperature and multiple reflow/high temperature aging. In: Proceedings of the International Symposium on Advanced Packaging Materials: Processes, Properties and Interfaces. IEEE, Washington, pp. 347–353.

Lin, J.K., Silva, A.D., Frear, D., Guo, Y., Hayes, S., Jang, J.W., Li, L., Mitchell, D., Yeung, B., Zhang, C., 2002. Characterization of lead-free solders and under bump metallurgies for flip-chip package. IEEE Transactions on Electronics Packaging Manufacturing 25, 300–307.

Nadai, A., 1950. Theory of Flow and Fracture of Solids. McGraw-Hill, New York.

Ricky Lee, S.W., Huang, X., 2002. Analysis on solder ball shear testing conditions with a simple computational model. Soldering and Surface Mount Technology 14, 45–48.

Shiau, L.C., Ho, C.E., Kao, C.R., 2002. Reactions between Sn–Ag–Cu lead-free solders and the Au/Ni surface finish in advanced electronic packages. Soldering and Surface Mount Technology 14, 25–29.

Towashiraporn, P., Gall, K., Subbarayan, G., McIlvanie, B., Hunter, B.C., Love, D., Sullivan, B., 2004. Power cycling thermal fatigue of Sn–Pb solder joints on a chip scale package. International Journal of Fatigue 26, 497–510.

Yoon, J.W., Kim, S.W., Jung, S.B., 2004. IMC growth and shear strength of Sn–Ag–Bi–In/Au/Ni/Cu BGA joints during aging. Materials Transactions 45, 727–733.

Yoon, J.W., Lee, C.B., Jung, S.B., 2003. Growth of an intermetallic compound layer with Sn–3.5Ag–5Bi on Cu and Ni–P/Cu during aging treatment. Journal of Electronic Materials 32, 1195–1202.

Zhao, X., Wang, C., Wang, G., Zheng, G., Yang, S., 2000. An integrated system for prediction and analysis of solder interconnection shapes. IEEE Transactions on Electronics Packaging Manufacturing 23, 87–92.